



Cite this: DOI: 10.1039/c9ee03566d

Received 4th November 2019,
Accepted 10th December 2019

DOI: 10.1039/c9ee03566d

rsc.li/ees

Blue energy fuels: converting ocean wave energy to carbon-based liquid fuels *via* CO₂ reduction†

Siu-Fung Leung,^a Hui-Chun Fu,^a Maolin Zhang,^a Ali H. Hassan,^a Tao Jiang,^b Khaled N. Salama,^a Zhong Lin Wang^c and Jr-Hau He^d *^{ad}

Sequestering CO₂ in the form of carbon-based liquid fuels would provide both a convenient and sustainable form of energy for practical use as well as mitigate the effects of global warming and climate change. Ocean wave energy is an abundant and relatively stable source of renewable energy, which would be highly desirable for the conversion of CO₂ to conveniently stored and transported liquid fuels. In this work, we demonstrate a wave-energy-driven electrochemical CO₂ reduction system, consisting of triboelectric nanogenerators, a supercapacitor and a CO₂ reduction reactor, that converts ocean wave energy to chemical energy in the form of formic acid, a liquid fuel. We optimize the energy storage component of the system and operation voltage of the electrochemical cell to achieve efficient energy storage and maximize the production of formic acid. Under simulated waves, the system can produce 2.798 μmol of formic acid per day *via* the wave energy harvested from a water surface area of 0.04 m². Moreover, we have performed field tests in the Red Sea to demonstrate the practicality of such an electrochemical CO₂ reduction system. Finally, we present design guidelines for achieving a cost-effective, efficient, and large-scale wave-energy-driven CO₂ reduction system for liquid fuel production.

Introduction

Global atmospheric carbon dioxide (CO₂) levels have reached a record high of 400 ppm, generating severe concern about the

Broader context

While the oceans cover more than 70% of the earth's surface, more efforts need to be invested to unleash the potential of wave energy. Meanwhile, harnessing the wave energy to convert carbon dioxide in the atmosphere to carbon-based liquid fuel is of great interest for modern society to address both the need of renewable energy and the concern of climate change. This work presents an ocean wave energy-powered electrochemical system to reduce carbon dioxide and produce formic acid, which is a form of hydrogen fuel. The system mainly consists of three components which are a spherical spring-assisted triboelectric nanogenerator to convert the mechanical energy of the wave to electrical energy, a power management circuit with a supercapacitor to temporarily store the harvested electrical energy and an electrochemical setup to reduce carbon dioxide to formic acid. In particular, we optimize the charging process of the supercapacitor and the operation potential of the electrochemical cells to more effectively utilize the energy harvested from the nanogenerator and maximize the production of formic acid. At the end, an outlook is presented to discuss the future challenges in developing a practical wave energy-powered liquid fuel production system.

effects of this greenhouse gas on climate change.¹ Despite this, fossil fuels still account for the largest portion of global energy production, the consumption of which is the primary source of greenhouse gases on the planet.^{2,3} Additionally, the finite reserves of fossil fuels have motivated the need to develop alternative energy sources other than petroleum-based hydrocarbons. The electrochemical reduction reaction of CO₂ (CO₂RR) is an enticing approach for converting CO₂ to useful carbon-based liquid fuels to mitigate current energy and environmental needs.^{4–8} However, the CO₂RR driven by renewable and sustainable energies is still underexplored and remains an ongoing challenge.

Ocean wave energy is an abundant sustainable energy source that is less-influenced by weather conditions compared with other renewable energies, such as solar power. Roughly 71% of the Earth's surface is covered by ocean, and studies indicate that ocean waves generate at least 8000 terawatt-hours per year of electrical energy.^{9,10} Yet, ocean wave energy is not widely exploited due to several reasons. First, wave energy plants are

^a Computer, Electrical and Mathematical Sciences and Engineering, King Abdullah University of Science and Technology, Thuwal 23955-6900, Kingdom of Saudi Arabia

^b CAS Center for Excellence in Nanoscience, Beijing Key Laboratory of Micro-nano Energy and Sensor, Beijing Institute of Nanoenergy and Nanosystems, Chinese Academy of Sciences, Beijing 100083, China

^c School of Materials Science and Engineering, Georgia Institute of Technology, Atlanta, Georgia 30332-0245, USA

^d Department of Materials Science and Engineering, City University of Hong Kong, Hong Kong Special Administrative Region. E-mail: jrhouhe@cityu.edu.hk

† Electronic supplementary information (ESI) available. See DOI: 10.1039/c9ee03566d

often off-shore, which poses difficulties in connecting to the power grid. Second, severe weather conditions, such as storms, and corrosion by sea water can cause damage to the wave power generator, which increases the cost of wave energy. Moreover, typical wave energy converters based on electromagnetic generators (EMGs) are bulky and cannot float, requiring supporting platforms or to be fixed on the sea floor, which causes disturbance to marine life.^{10–12}

In an effort to overcome the problems associated with EMGs, triboelectric nanogenerators (TENGs), which are able to convert mechanical energy into electricity based on the effect of triboelectrification and electrostatic induction, have recently been employed for harvesting wave energy. TENGs feature a simple structure, and are light-weight, and made of low-cost materials, garnering increased interest in large-scale deployment as wave energy generators.^{10,13–23} A key advantage of the TENG over the EMG is that the power output of an EMG is proportional to the square of frequency of the motion, while the power output of TENG is proportional to the frequency. As a result, there exists a critical frequency (~ 5 Hz) and a TENG has a higher output below this critical frequency than the EMGs in the same scale, which makes the TENGs particularly suitable for wave energy harvesting considering that the frequency of ocean wave motion is often below 5 Hz.^{10,24} Various designs of TENGs had been studied to improve the power output of wave energy conversion, from 50 mW m^{-2} by liquid–solid electrification to 1.366 W m^{-2} in 2016.^{17,25} Additionally, these TENGs are able to naturally float on the water's surface, causing minimal impact to the environment.

Besides converting ocean wave energy to electricity, other applications of wave energy harvesting by TENGs have been explored, including wave-energy-powered water desalination and water splitting for hydrogen fuel production.^{9,26,27} Notably, converting wave energy to electrical energy and then storing that energy in chemical fuels is more desirable compared with energy storage by supercapacitors and batteries,^{28–30} as these devices suffer from self-discharge, resulting in energy loss, while chemical fuels do not and are relatively easy to store and transport. However, additional effort is required to optimize the power management and electrochemical aspects of such wave energy to chemical fuel conversion systems. In particular, formic acid (HCOOH) obtained by the electrochemical CO_2RR is preferable to pure hydrogen obtained by water splitting as a hydrogen storage medium^{27,31} because formic acid is liquid at room temperature, making it safer and easier to store and transport. In addition, it has a relatively high volumetric hydrogen density of $53 \text{ g of H}_2 \text{ per L}$. However, there are no reports of carbon-based liquid fuels produced by TENG-powered CO_2RR , which involves complicated electrochemical processes and requires more optimization.²⁶

Herein, we demonstrate liquid fuel production by electrochemical CO_2RR powered by ocean wave energy harvested using spring-assisted spherical TENGs.^{16,22} This type of TENG is more cost-effective compared to conventional EMG-based wave energy converters. Moreover, it features a higher wave energy conversion efficiency and power output as compared to

previous TENG designs and is able to float on the water's surface, which both minimizes the environmental impact and simplifies operation,^{16,22} and these features are essential for the practical use of TENGs in ocean wave energy harvesting applications. We optimize the operation parameters of this wave-energy-driven CO_2RR system, including the capacitance of the triboelectric charge storage device and the operation voltage of the electrochemical cell to achieve near 100% faradaic efficiency (FE) for the CO_2RR and maximize the liquid fuel product. When tested with a lab-simulated wave, the wave-energy-driven CO_2RR system can produce a maximum of $2.798 \mu\text{mol}$ of formic acid per day by TENGs on a water surface area of 0.04 m^2 . Furthermore, we performed field tests in the Red Sea under different wind speed conditions to study the practical performance of the CO_2RR system. According to our field test results, the wave-energy-driven CO_2RR system can produce $0.325 \mu\text{mol}$ of formic acid per day at 18 knots wind speed. Finally, we present an outlook for the future development of liquid fuel production by wave energy. Our work not only demonstrates the first ever reported production of a carbon-based liquid fuel by a wave-energy-driven CO_2RR system, but also optimizes the system parameters and provides important design guidelines for maximizing the liquid fuel product.

Results and discussion

Design of the wave-energy-driven CO_2RR system

Fig. 1 shows a detailed schematic of the wave-energy-driven CO_2RR system. The system consists of three major components, including the spring-assisted TENG for converting wave energy to electricity, a power management circuit consisting of bridge rectifiers and a supercapacitor, and a two-electrode electrochemical cell responsible for the CO_2RR and oxygen evolution reaction (OER). The detailed equivalent circuit diagram of the system can be found in Fig. S1 (ESI[†]). An optical image of the spherical TENG used is shown in Fig. S2a (ESI[†]), the fabrication details of which can be found in our previous studies.^{16,22} As shown in Fig. 1, the outer shell of the TENG is made of acrylic. Inside the sphere, there are two regions separated by three circular acrylic plates and supported by four springs. The TENG is located in the bottom region of the device and the top region serves as a buffer, which allows the underlying TENG to be compressed and decompressed. The TENG itself is a folded, multi-layered structure that maximizes the contact area between aluminum and fluorinated ethylene propylene (FEP) films. During compression, electrons transfer from the aluminum to the more electron-attracting FEP, and the resulting triboelectric charges are conducted away. Moreover, the four springs in the design enable kinetic energy from a wave to be stored and converted to electricity from the residual vibration of the springs. In our experiments, we connected four spherical TENGs in parallel to increase the power output. The spherical TENGs are connected externally to a circuit board that consists of bridge rectifiers for converting the alternating current from the TENG to direct current, as well as a supercapacitor to temporarily store the triboelectricity

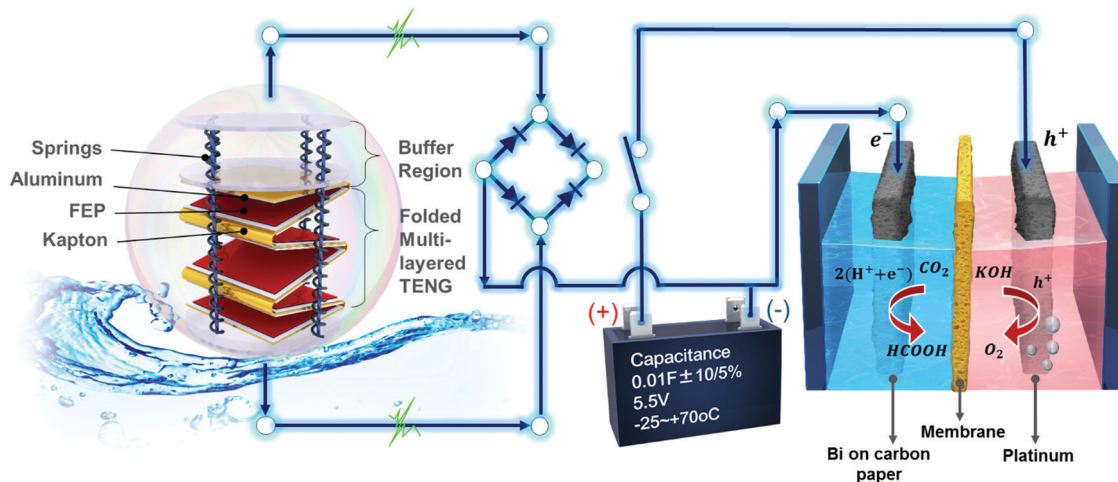


Fig. 1 Schematic of the ocean-wave-driven electrochemical CO₂RR system for liquid fuel production. The system consists of three components: the spring-assisted spherical TENG; an energy storage circuit with rectifiers and a supercapacitor; and a two-electrode electrochemical cell for CO₂RR and OER.

produced. The supercapacitor plays two important roles in the system. First, the power output of the TENG is pulsed, and the supercapacitor acts as a reservoir of triboelectricity and provides a steady power output for electrochemical reactions when discharging. Second, it can accommodate the optimal operation potential of electrochemical cells. This is because the typical voltage output of TENGs can reach over a hundred volts and it is too high and inefficient for electrochemical reactions if the TENG is just directly connected to the electrochemical cells without the use of a supercapacitor.

Optimization of the triboelectric charge storage

When the supercapacitor is charged to a sufficient voltage by the TENGs, it connects to a gas-tight two-electrode electrochemical cell and drives the OER and CO₂RR, with the positive terminal connected to the anode and the negative terminal connected to the cathode. The catalyst and electrolyte for the OER are platinum (Pt) foil and 1 M potassium hydroxide (KOH), and those for CO₂RR are bismuth(III) oxide (Bi₂O₃) and 0.5 M CO₂-saturated potassium bicarbonate (KHCO₃), respectively. Further experimental details of the electrochemical cell catalysts can be found in the Methods section. Fig. S2 (ESI[†]) shows a photograph of the gas-tight two-electrode electrochemical cell. In this work, we adopt the fabrication of a Bi₂O₃ catalyst reported in the literature,⁵ and it shows that the major CO₂RR product by the Bi₂O₃ catalyst is formic acid with a negligible amount of carbon monoxide and hydrogen. The CO₂RR and OER can be represented by the following chemical equations, in which formate is produced on the cathode by the CO₂RR.



Fig. 2a shows the uncorrected linear sweep voltammetry (LSV) curves of the CO₂RR on the Bi₂O₃-coated cathode in 0.5 M

KHCO₃ (Blue curve) and the OER on the Pt anode in 1 M KOH (red curve) carried out with a potentiostat at a scan rate of 10 mV s⁻¹. If we take the onset potential for both CO₂RR and OER at 1 mA cm⁻², then the onset voltage to drive both reactions is ~1.9 V. In the wave-energy-driven CO₂RR system, the role of the capacitor is to temporarily store the triboelectricity generated by the TENGs and drive the CO₂RR and OER when it reaches a sufficient voltage. Therefore, the capacitor will be charged to a certain voltage above 1.9 V by the TENGs, after which it discharges to drive the CO₂RR and OER, and eventually stops discharging when the capacitor voltage drops to 1.9 V. This process is one operation cycle of the wave-energy-driven CO₂RR system. In regards to the capacitance, on the one hand, it must be large enough to provide sufficient energy and sustain a reasonable period of discharging time for the electrochemical reactions, particularly for the sluggish OER.^{32,33} On the other hand, if the capacitance is too large, it will take too long to charge to the required voltage for the electrochemical reactions. Therefore, we tested the system with capacitors that ranged from 100 μF to 0.1 F in capacitance and analyzed the liquid products of the electrochemical reactions by nuclear magnetic resonance (NMR). We detected no liquid product when the capacitance was lower than 0.01 F, which is due to the insufficient charge to sustain a reasonable discharging time. Therefore, we searched for a suitable capacitance value within a range of 0.01–0.1 F.

Fig. 2b and c are the voltage and stored energy against charging time for the capacitors ranging from 0.01 F to 0.1 F when charged by four spherical TENGs connected in parallel. The four spherical TENGs have a projected area on the water's surface of 0.04 m² (20 × 20 cm²) and were powered by a simulated wave that mainly drove the TENGs up and down (see Methods for more details). Under this wave, the 0.01 F capacitor reaches 0.5 V in less than 600 s, while the 0.1 F capacitor can only reach 0.042 V in the same period of time. Furthermore, the stored energy in the 0.01 F capacitor is 14 times

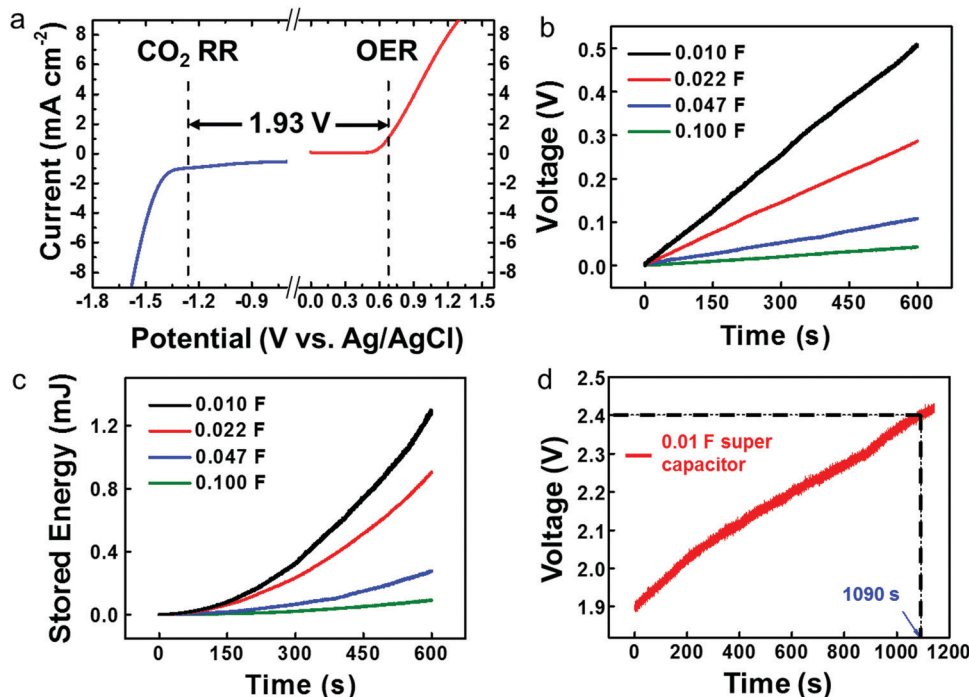


Fig. 2 Characterization of the electrochemical reactions and the supercapacitor charging by the TENGs. (a) LSV curves of the CO₂RR on the Bi₂O₃-coated cathode in 0.5 M CO₂-saturated KHCO₃ (blue curve) and the OER on the Pt anode in 1 M KOH (red curve) at a scan rate of 10 mV s⁻¹. (b) Voltage and (c) stored energy against charging time for capacitors that ranged from 0.01 F to 0.1 F when charged by four spherical TENGs connected in parallel. (d) Voltage against charging time when charging the 0.01 F supercapacitor from 1.9 V to 2.4 V by the TENGs.

higher than that in the 0.1 F device, despite being charged in the same way. This phenomenon can be explained by the better impedance matching between the load capacitance and the inherent capacitance of the TENG, which results in higher energy storage efficiency, which has been studied in detail in our previous studies.^{34,35} As a result, we chose the 0.01 F capacitor to store the generated triboelectricity because of its higher energy storage efficiency. It is worth noting that a supercapacitor is more suitable as charge storage than a Li-ion battery in this work since the power capacity of the TENG in this work is insufficient to charge a Li-ion battery. Despite this, we suggest that Li-ion batteries can be used when the size and power capacity of such a system are scaled up in the future.

Optimization of the operation voltage of the two-electrode electrochemical cell

As previously noted, 1.9 V is the minimum voltage needed to drive both the CO₂RR and OER. However, we still needed to determine the voltage at which the capacitor should be charged in order to yield the most formic acid. While a higher discharge voltage should produce more formic acid in each discharge cycle, it takes longer to charge. To explore this tradeoff, we charged the capacitor to a range of voltages, including 2.4 V, 2.9 V, and 3.9 V (corresponding to 0.5 V, 1 V, and 2 V higher than 1.9 V) and analyzed the amount of liquid products produced by these discharge voltages (V_{dis}). Fig. 2d displays the capacitor voltage against charging time, in which the spherical TENGs driven by the simulated wave require

~1090 s to charge a 0.01 F capacitor from 1.9 V to 2.4 V, and ~2468 s and ~7424 s to charge the capacitor from 1.9 V to 2.9 V and 1.9 V to 3.9 V, respectively. The capacitor voltage increases more slowly at higher voltages, which is a typical behavior of capacitor charging.³⁵ Fig. S3 (ESI[†]) shows the self-discharge characteristics of the 0.01 F supercapacitor after being charged to 2.4 V. We observe a notable self-discharge as the voltage drops to 2.32 V in 0.5 h, and then drops below 1.6 V in 24 h, clearly demonstrating the advantage of converting wave energy to chemical fuels over storing the harvested wave energy in supercapacitors/batteries.

Fig. 3a and b show the voltage and current characteristics over time when the 0.01 F capacitor is discharged at 3.9 V, 2.9 V, and 2.4 V to drive the two-electrode electrochemical cell. In all cases, the current rises rapidly to approximately 10–15 mA and then drops to below 1 mA in 5 s. The entire discharge cycle in all cases finishes in ~20 s. From the voltage characteristics, we can observe that the beginning of the recorded voltage never reaches the discharge voltages (3.9 V, 2.9 V and 2.4 V), though the data acquisition is at 10 Hz. That means the capacitor voltage drops very rapidly at the beginning of the discharge process, especially when discharging at 3.9 V, and it drops below 2.9 V in less than 1 s because of the high current density at the high over potential as shown in Fig. 2a.

Using NMR, we quantitatively analyzed the liquid products of the CO₂RR after being driven by the three discharge voltages. In order to ensure there was a detectable amount of liquid

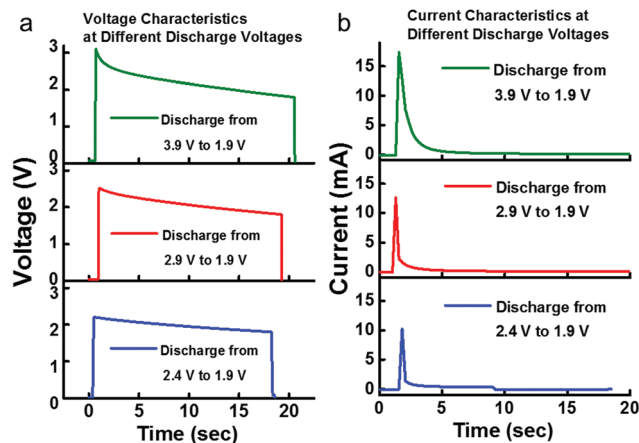


Fig. 3 (a) Voltage and (b) current characteristics of the supercapacitor when discharging to the two-electrode electrochemical cell at 3.9 V, 2.9 V, and 2.4 V.

product in the resulting solution for each condition, we conducted multiple charge–discharge cycles for each voltage over the course of an hour. The details of the experiment and NMR analysis can be found in the Methods section. From the NMR analysis, we can only detect formic acid as the major liquid product. The average FEs of the three V_{dis} calculated from the result of NMR are shown in Fig. 4a (the corresponding statistics are shown in Table S1, ESI†). The 3.9 V V_{dis} featured the lowest average FE of 76%. When discharging at a lower voltage, the average FE increases to 96% for 2.9 V V_{dis} and reaches the highest FE of nearly 100% when discharged at 2.4 V, which agrees with the FEs at the similar potential reported in the literature.⁵ The higher FE from the lower discharge voltage can be explained by the following reasons. First, the higher over potential will result in increased production of other chemical products, such as hydrogen for the Bi_2O_3 catalyst.⁵ Second, the high voltage region (3.9 V to 2.9 V) is sustained for only a very short period of time as described previously in Fig. 3. Therefore, the discharging time may be too short to allow all the charges produced to contribute to the anodic and cathodic electrochemical reactions, particularly in the case of the sluggish OER.^{32,33} During the experiment, we also tried to analyze the gaseous product by gas chromatography, however, we were not able to obtain a reliable result, possibly due to the deficient amount of gaseous product. It is worth noting that we did not get detectable electrochemical product for V_{dis} effectively below 2.4 V, which might be due to the insufficient amount of energy stored in the supercapacitor to power up the electrochemical reaction. Despite this, here shows an important rule to improve the utilization of electric charge when powering up electrochemical reactions using capacitors.

Fig. 4b shows the amount of formic acid produced per cycle by the three discharge voltages, which are measured by NMR. As expected, discharging at 3.9 V produces the most formic acid per cycle at $0.067 \mu\text{mol}$ per 0.57 mg cm^{-2} of catalyst loading, while discharging at 2.9 V and 2.4 V produces $0.047 \mu\text{mol}$ and

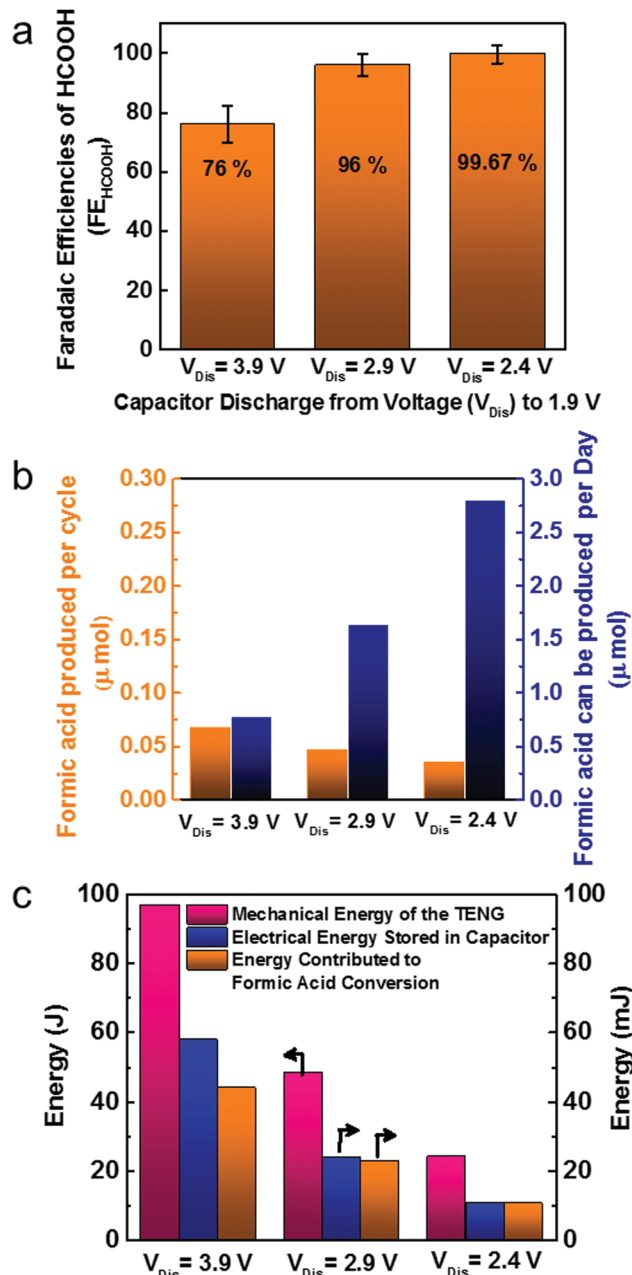


Fig. 4 Analysis of the chemical product by NMR and energy conversion efficiencies. (a) Faradaic efficiencies of formic acid when the capacitor discharge was at 3.9 V, 2.9 V, and 2.4 V. (b) Amount of formic acid that can be produced per cycle and per day at the three discharge voltages. (c) Estimate of the energy conversion efficiencies from the mechanical energy of the TENGs to the energy contributed to formic acid conversion.

$0.035 \mu\text{mol}$ of formic acid, respectively. Interestingly, when we estimate the amount of formic acid produced per day by evaluating how many cycles can be undergone in 24 h, we found that discharging at 2.4 V can yield the most formic acid of $2.798 \mu\text{mol}$ per day while discharging at 2.9 V and 3.9 V can only produce $1.635 \mu\text{mol}$ and $0.777 \mu\text{mol}$, respectively. This intriguing result can be attributed to the lower charging efficiency at higher capacitor voltage and the lower faradaic efficiency when discharging at 3.9 V, as we discussed earlier.

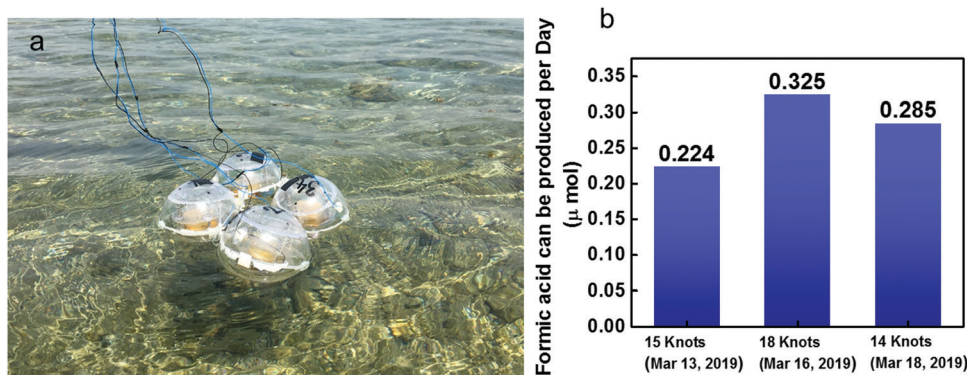


Fig. 5 Field test of the wave-energy-driven CO₂RR system. (a) Photograph of the field test showing the four spherical TENGs connected in parallel to charge the 0.01 F supercapacitor by ocean waves. (b) The amount of formic acid that can be produced per day at different wind speeds.

Therefore, we can conclude that it is beneficial to charge the capacitor to a lower voltage above the onset potential in terms of the daily amount of formic acid production. It is worth noting that although the amount of formic acid produced seems small, it is made by TENGs featuring a total area of only 0.04 m². The light-weight, low-cost, and low environmental disturbance of the spherical TENGs suggest that our wave-energy-driven CO₂RR system could be highly advantageous in large-scale deployment as compared with conventional wave energy converters based on EMGs.

Besides studying the chemical products, we also evaluated the efficiencies of the entire energy conversion process, from the kinetic energy of the TENGs to the energy being consumed to reduce CO₂ to formic acid. Fig. 4c and Table S2 (ESI[†]) demonstrate the energies obtained at different stages of the conversion process for the three discharge voltages, including the mechanical energy of the TENGs, the electrical energy stored in the capacitor, and the energy contributed to the formic acid conversion in each cycle. For the mechanical energy of the TENGs, we assumed they displayed simple harmonic motion under the influence of the water wave and estimated the average kinetic energy in one cycle of charging by $\frac{1}{4}m(2\pi f)^2a^2$, in which m is the mass of the TENGs, and f and a are the frequency and the amplitude of the simple harmonic motion, respectively. The details of the calculations can be found in the Methods section. From the plot in Fig. 4c, we can see a significant energy loss in the mechanical to electrical energy conversion, which can be explained by the non-optimized impedance between the TENGs and the 0.01 F capacitor, leading to inefficient energy transfer. The need for the capacitance to balance the charging time and the energy stored poses a constraint on the choice of the capacitance and the optimization between the load capacitance and the inherent capacitance of the TENG. In addition, the design of the spherical TENG can be further improved to enhance the power output, such as by increasing the number of triboelectric layers to fully utilize the space inside the sphere. In contrast to the mechanical to electrical energy conversion, the electrical to chemical energy conversion is very effective thanks to the high FE of formic acid, as shown in Fig. 4a. Meanwhile, this also suggests that there is little issue in

the conversion loss when we substitute capacitors/batteries with chemical fuels as energy storage media.

Field test

To demonstrate the practicality of the wave-energy-driven CO₂RR system, we performed field tests in the Red Sea at the shore of our university (location at N 22°20'31.232" and E 39°05'17.307"). Fig. 5a and Video S1 (ESI[†]) show a photograph and video of the field test. The tests were performed on March 13, March 16, and March 18, 2019 when the wind speeds at 3 pm were 15 knots, 18 knots, and 14 knots, respectively. During the tests, the multi-layered structures in the spherical TENGs were compressed and decompressed as the devices moved in the water, converting the wave energy to electrical energy stored in the 0.01 F capacitor. We measured the voltage charged in 1 h, and then calculated the time needed to charge the 0.01 F capacitor from 1.9 V to 2.4 V and the amount of formic acid that theoretically could be produced by the CO₂RR system on the three test days (Fig. 5b). Overall, we can see that more formic acid can be produced on a windier day. We note that the capacitor charging in the sea is slower than that in the lab-simulated wave. This is attributed to our observation that the motion of the TENGs on the sea is rather orbital, with both vertical and lateral motion instead of the mainly vertical motion experienced in the simulated wave. As a result, the vertically-stacked multi-layered TENG cannot fully utilize the wave energy in the sea.

Conclusions

In conclusion, we demonstrate an ocean wave-energy-driven electrochemical CO₂RR system that converts wave energy to conveniently stored and transported carbon-based liquid fuels. The spring-assisted TENGs, which can convert the energy of a wave to electricity stored in a capacitor, are low-cost, light-weight, and cause less disturbance to marine life. The stored energy can then be used to convert CO₂ to formic acid *via* electrochemical reduction. Moreover, we have optimized the system's parameters, including the capacitance of the triboelectric charge storage and operation voltage of the CO₂RR system so that optimal energy storage and formic acid

conversion efficiencies are achieved. Our findings show that setting the discharge voltage of the capacitor, which temporarily stores the triboelectricity, at an optimal value of 2.4 V for each cycle, results in an FE of nearly 100% for the conversion of CO₂ to formic acid. The CO₂RR system can produce 2.798 μmol of formic acid per day with wave energy harvested from an area of 0.04 m². Additionally, we tested the wave-energy-driven CO₂RR system in real conditions to demonstrate the practicality of converting ocean wave energy to liquid fuels. To the best of our knowledge, this is the first demonstration of a wave-energy-driven CO₂RR system that can simultaneously convert CO₂, a major greenhouse gas, to carbon-based liquid fuel using abundant ocean wave energy.

Outlook

From our estimates based on the experimental results, we believe that a wave-energy-driven CO₂RR system installed with 1 km² of TENGs can generate about 56% of the daily per capita energy consumption in the world (according to 2015 data, see calculation in the ESI†). Nonetheless, there is still room for improvement in the energy conversion efficiency of the system. While the major components, including the TENGs, power management circuit, electrochemical cell, and catalysts, are all fairly mature, substantial optimization is still needed when combining them for an efficient wave-energy-driven CO₂RR system. First, the energy storage efficiency should be improved by better matching the impedance between the TENGs and the energy storage components. Despite extensive research on improving the charging efficiency of the capacitor by the TENGs,^{34,35} further studies are still needed since the load capacitance of the capacitor and inherent capacitance of the TENG will depend on the targeted energy production and TENG design. In addition, Zi *et al.* have reported that the designed charging cycle can significantly improve the energy-storage efficiency up to 50%. The higher energy-storage efficiency is essential for practical use of TENGs to harvest ambient mechanical energies.³⁶ Second, in order to deliver a higher power output and more effectively utilize the ocean wave energy, the design of the TENG must be further improved to better accommodate the actual dynamics of ocean waves rather than a lab-simulated wave. As a matter of fact, researchers keep investing their effort to achieve higher performance in harvesting ambient mechanical energy by TENGs. For example, when we were preparing this communication, Li *et al.* reported an Oblate Spheroidal TENG which consists of two TENG parts that can better adapt to both rough and quiet sea conditions. The design has also considered the actual dynamic of the ocean wave, which can more effectively convert the vertical and horizontal motions of the ocean wave into electrical energy.²³ Third, system integration plays a key role in the performance of such a wave energy-driven CO₂ reduction system. In the past, components utilized in our system including TENGs, power management circuits and the catalysts for electrochemical reactions were characterized and optimized separately with the best performance revealed in their optimal working conditions. However, there are substantial

challenges when integrating these components to achieve the best performance of the system. Taking this work as an example, the voltage output generated by the TENG is pulsed and too high for typical electrochemical reactions, which requires a supercapacitor for temporary charge storage. And we found that the faradaic efficiency is largely dependent on the operation voltage of the electrochemical cells. We foresee that substantial works must be carried out in the future to achieve practical use of such a wave energy harvesting system. For example, when advancing the design and scaling up the power output of TENGs, the inherent impedance will vary which can significantly alter the optimal charging condition for the energy storage device. Besides, scaling up the effective area of the TENG will unavoidably largely increase the size and the physical distance between the TENGs and power management unit, which will introduce problems such as loss of energy in the connection between the components and these problems need substantial efforts to overcome. Finally, besides the above, the cost of fabricating the TENGs must be lowered, and it should be made more convenient to form a large network of TENGs to deliver cheaper and higher wave power output.

Methods

Charging performance measurements by the TENG array

Four spherical TENGs with the spring-assisted multilayered structure are respectively connected to a full-bridge rectifier and then connected in parallel. The TENGs are then used to charge various super-capacitors under the water waves generated by using a series of wave pumps (rw-20 JEPOWER TECHNOLOGY Inc.) controlled by a function generator (AFG3011C Tektronix Inc.). The output frequency and output amplitude of the function generator are set as 1.0 Hz and 2.5 V, respectively. The capacitances ranged from 0.01 F to 0.1 F. The voltage on the supercapacitors is measured by a current preamplifier (Keithley 6514 System Electrometer). Note that when charging the super-capacitor from 1.9 V by the TENGs, we first charged it from 0 to 1.9 V by using the direct-current power source.

Preparation of the two-electrode electrochemical cell, catalyst and linear sweep voltammetric (LSV) measurement

To prepare the cathodic electrode, 5 mg of the obtained Bi₂O₃ nanosheet powder was dispersed in 750 μl of ethanol, 250 μl of deionized water and 40 μl of 5 wt% Nafion solution with sonication for 30 min, and then 120 μl of the mixed solution was dropped on 1 × 1 cm⁻² carbon paper and dried at room temperature. The loading amount of the catalyst is 0.57 mg cm⁻². An electrocatalytic experiment was carried out with a potentiostat (Biologic-SAA) in a two-electrode electrochemical cell (optical images are shown in Fig. S2b and c, ESI†), and a bipolar membrane was used to separate the anodic and cathodic compartments. The catalyst loaded carbon paper and Ag/AgCl (saturated KCl solution) were placed in the cathodic side, and used as a working and reference electrode, respectively. A platinum wire electrode was used as the counter electrode in the anodic side. For the cathodic compartment, 0.5 M KHCO₃ electrolyte was used, while the

anodic compartment was 1 M KOH electrolyte, each compartment containing 9 ml electrolyte with a 3 ml headspace. The cathodic

following equations are used to calculate the faradaic efficiency of CO₂ reduction gaseous products.

$$\begin{aligned} \text{FE}_{\text{gaseous}} \% &= \frac{Q_i}{Q_{\text{total}}} \times 100\% = \frac{Z_i \times P_0 \times V_0 \times v (\text{vol}\%) \times F}{R \times T \times I \times 60 (\text{s min}^{-1})} \\ &= \frac{2 \times 1.013 \times 10^5 (\text{Pa}) \times V_0 (\text{ml min}^{-1}) \times 10^{-6} (\text{m}^3 \text{ml}^{-1}) \times v (\text{vol}\%) \times 96\,485 (\text{C mol}^{-1})}{8.314 (\text{m}^3 \text{Pa mol}^{-1} \text{K}^{-1}) \times 298 (\text{K}) \times I (\text{C s}^{-1}) \times 60 (\text{s min}^{-1})} \end{aligned}$$

electrolyte was pre-saturated with Ar or CO₂ (99.999%) with an average flow rate of 10 sccm for 30 min before CO₂ reduction. The pH of the CO₂ saturated electrolyte was measured as 7.34. For the preparation of catalysts, we adopt the fabrication of the catalyst reported here.⁵ CV and polarization curves were collected (no iR-corrected) at a scan rate of 10 mV s⁻¹ using a potentiostat (Biologic-SAA). Before the test, the Bi₂O₃ loaded electrode was biased at -1.6 V vs. Ag/AgCl for 1 h to Bi metal. The reduced working electrode was taken out of the electrolyte, rinsed with deionized water and immersed in fresh 0.5 M KHCO₃. When testing the CO₂RR at the three discharge voltages, we carried out multiple charge-discharge cycles for each voltage in an hour to ensure a detectable amount of liquid product in the resulting solution. Thereafter, the liquid products in the resulting solution were analyzed by NMR.

Nuclear magnetic resonance and gas chromatography for the CO₂RR product

To analyze the liquid product, 600 MHz ¹H nuclear magnetic resonance (NMR) spectroscopy was used. After each electrolysis at a fixed potential, 510 μl of electrolyte was taken out and transferred to the NMR sample tube. Then 10 μl of an internal standard, which contains 0.05 mmol l⁻¹ dimethyl sulfoxide (DMSO) and 120 μl D₂O was added. The ¹H spectrum was obtained with water suppression using a presaturation method. Here, HCOOH is the only liquid product. The following equations are used to calculate the faradaic efficiency of HCOOH.

$$\text{FE}_{\text{liquid}} \% = \frac{Q_{\text{HCOOH}}}{Q_{\text{CA}}} \times 100\% = \frac{2 \times N_{\text{HCOOH}} \times F}{Q_{\text{CA}}}$$

N_{HCOOH} is the number of moles of HCOOH in the cathodic electrolyte, which is calibrated by the standard calibration curve from a series of standard HCOOH solutions. Q_{CA} is the total charge passing through the electrode during electrolysis, which is calculated by integrating the plot of chronoamperometry (CA). Since we have performed multiple charge-discharge cycles for the three discharge voltages in one hour, the amount of liquid product obtained per cycle is calculated by the total amount of liquid product divided by the number of cycles undergone.

The gaseous products (H₂ and CO) were detected by an online gas chromatograph (Agilent 7890 B) equipped with a Shincarbon Column, thermal conductivity detector (TCD) and flame ionization detector (FID) with a methanizer used for H₂ and CO quantification, respectively. Ultrahigh purity Ar (99.999%) was used as the carrier gas. The volume ratio of gaseous products was calibrated by standard curves from standard gases. The

Here, Z_i is the number of electrons needed for reducing CO₂ to H₂ or CO, both H₂ and CO need 2 electrons; P_0 is the pressure, V_0 is the gas flow rate measured by a flow meter, v (vol%) is the volume ratio of H₂ or CO in the GC sampling loop, F is the faradaic constant (96 485 C mol⁻¹), R is the ideal gas constant (8.314 m³ Pa mol⁻¹ K⁻¹), T is the reaction temperature (298 K), and I is the average current during the sample injection.

Estimation of the energy conversion efficiency

For the mechanical energy of the TENGs, we assume the simple harmonic motion (SHM) of the TENGs under the influence of a water wave. And the mechanical energy of the TENGs to charge the capacitor is estimated by the average kinetic energy in one cycle of SHM multiplied by the time needed to charge to the specific voltage, which equals to $\frac{1}{4}m(2\pi f)^2 a^2 \times T$ where m is the mass of the TENGs, f and a are the frequency and the amplitude of the SHM, and T is the charging time, which is 1090 s, 2468 s and 7424 s to charge a 0.01 F capacitor from 1.9 V to 2.4 V, 2.9 V and 3.9 V, respectively. The energy stored in the capacitor is calculated by $\frac{1}{2}CV^2$, where C is the capacitance and V is the capacitor voltage. The energy contributed to the conversion of formic acid is calculated by energy stored in the capacitor multiplied by the faradaic efficiency.

Author contribution

S.-F. L. and J.-H. H. conceived the project, designed the experiments, and wrote the manuscript. H.-C. F. and M. Z. performed the electrochemical experiments. A. H. H. fabricated the power management circuit. T. J. fabricated and characterized the TENGs. All authors discussed the results and gave comments on the paper.

Conflicts of interest

The authors declare no competing interests.

Acknowledgements

This work was financially supported by the Office of Sponsored Research of King Abdullah University of Science and Technology (KAUST), the KAUST Sensor Initiative and the City University of Hong Kong startup funding.

References

- N. Jones, *Nat. Geosci.*, 2013, **6**, 589.
- C. Breyer, D. Bogdanov, A. Aghahosseini, A. Gulagi, M. Child, A. S. Oyewo, J. Farfan, K. Sadovskaia and P. Vainikka, *Prog. Photovoltaics*, 2018, **26**, 505–523.
- C. McGlade and P. Ekins, *Nature*, 2015, **517**, 187–190.
- Y. H. Wang, J. L. Liu, Y. F. Wang, Y. G. Wang and G. F. Zheng, *Nat. Commun.*, 2018, **9**, 5003.
- C. W. Lee, J. S. Hong, K. D. Yang, K. Jin, J. H. Lee, H. Y. Ahn, H. Seo, N. E. Sung and K. T. Nam, *ACS Catal.*, 2018, **8**, 931–937.
- N. Han, Y. Wang, H. Yang, J. Deng, J. H. Wu, Y. F. Li and Y. G. Li, *Nat. Commun.*, 2018, **9**, 1320.
- F. Yang, P. Song, X. Z. Liu, B. B. Mei, W. Xing, Z. Jiang, L. Gu and W. L. Xu, *Angew. Chem., Int. Ed.*, 2018, **57**, 12303–12307.
- W. Y. Zhang, Q. Qin, L. Dai, R. X. Qin, X. J. Zhao, X. M. Chen, D. H. Ou, J. Chen, T. T. Chuong, B. H. Wu and N. F. Zheng, *Angew. Chem., Int. Ed.*, 2018, **57**, 9475–9479.
- J. Leijon and C. Bostrom, *Desalination*, 2018, **435**, 161–171.
- Z. L. Wang, T. Jiang and L. Xu, *Nano Energy*, 2017, **39**, 9–23.
- A. F. D. Falcao, *Renewable Sustainable Energy Rev.*, 2010, **14**, 899–918.
- J. Falnes, *Mar. Struct.*, 2007, **20**, 185–201.
- S. F. Leung, K. T. Ho, P. K. Kung, V. K. S. Hsiao, H. N. Alshareef, Z. L. Wang and J. H. He, *Adv. Mater.*, 2018, **30**, 1704611.
- L. M. Zhang, C. B. Han, T. Jiang, T. Zhou, X. H. Li, C. Zhang and Z. L. Wang, *Nano Energy*, 2016, **22**, 87–94.
- X. F. Wang, S. M. Niu, Y. J. Yin, F. Yi, Z. You and Z. L. Wang, *Adv. Energy Mater.*, 2015, **5**, 1501467.
- T. Jiang, Y. Y. Yao, L. Xu, L. M. Zhang, T. X. Xiao and Z. L. Wang, *Nano Energy*, 2017, **31**, 560–567.
- A. Ahmed, Z. Saadatnia, I. Hassan, Y. L. Zi, Y. Xi, X. He, J. Zu and Z. L. Wang, *Adv. Energy Mater.*, 2017, **7**, 1601705.
- T. X. Xiao, T. Jiang, J. X. Zhu, X. Liang, L. Xu, J. J. Shao, C. L. Zhang, J. Wang and Z. L. Wang, *ACS Appl. Mater. Interfaces*, 2018, **10**, 3616–3623.
- L. Pan, J. Y. Wang, P. H. Wang, R. J. Gao, Y. C. Wang, X. W. Zhang, J. J. Zou and Z. L. Wang, *Nano Res.*, 2018, **11**, 4062–4073.
- K. Lee, J. W. Lee, K. Kim, D. Yoo, D. S. Kim, W. Hwang, I. Song and J. Y. Sim, *Micromachines*, 2018, **9**, 598.
- Z. H. Lin, G. Cheng, S. Lee, K. C. Pradel and Z. L. Wang, *Adv. Mater.*, 2014, **26**, 4690–4696.
- T. X. Xiao, X. Liang, T. Jiang, L. Xu, J. J. Shao, J. H. Nie, Y. Bai, W. Zhong and Z. L. Wang, *Adv. Funct. Mater.*, 2018, **28**, 1802634.
- G. Liu, H. Guo, S. Xu, C. G. Hu and Z. L. Wang, *Adv. Energy Mater.*, 2019, **9**, 1900801.
- C. Zhang, W. Tang, C. B. Han, F. R. Fan and Z. L. Wang, *Adv. Mater.*, 2014, **26**, 3580–3591.
- G. Zhu, Y. J. Su, P. Bai, J. Chen, Q. S. Jing, W. Q. Yang and Z. L. Wang, *ACS Nano*, 2014, **8**, 6031–6037.
- W. Tang, Y. Han, C. B. Han, C. Z. Gao, X. Cao and Z. L. Wang, *Adv. Mater.*, 2015, **27**, 272–276.
- Y. Yang, H. L. Zhang, Z. H. Lin, Y. Liu, J. Chen, Z. Y. Lin, Y. S. Zhou, C. P. Wong and Z. L. Wang, *Energy Environ. Sci.*, 2013, **6**, 2429–2434.
- P. Varadhan, H. C. Fu, D. Priante, J. R. D. Retamal, C. Zhao, M. Ebaid, T. K. Ng, I. Ajia, S. Mitra, I. S. Roqan, B. S. Ooi and J. H. He, *Nano Lett.*, 2017, **17**, 1520–1528.
- W. J. Li, H. C. Fu, Y. Z. Zhao, J. H. He and S. Jin, *Chem*, 2018, **4**, 2644–2657.
- G. Glenk and S. Reichelstein, *Nat. Energy*, 2019, **4**, 216–222.
- J. Eppinger and K. W. Huang, *ACS Energy Lett.*, 2017, **2**, 188–195.
- N. T. Suen, S. F. Hung, Q. Quan, N. Zhang, Y. J. Xu and H. M. Chen, *Chem. Soc. Rev.*, 2017, **46**, 337–365.
- M. Tahir, L. Pan, F. Idrees, X. W. Zhang, L. Wang, J. J. Zou and Z. L. Wang, *Nano Energy*, 2017, **37**, 136–157.
- Y. Y. Yao, T. Jiang, L. M. Zhang, X. Y. Chen, Z. L. Gao and Z. L. Wang, *ACS Appl. Mater. Interfaces*, 2016, **8**, 21398–21406.
- S. M. Niu, Y. Liu, Y. S. Zhou, S. H. Wang, L. Lin and Z. L. Wang, *IEEE Trans. Electron Devices*, 2015, **62**, 641–647.
- Y. Zi, J. Wang, S. Wang, S. Li, Z. Wen, H. Guo and Z. L. Wang, *Nat. Commun.*, 2016, **7**, 10987.